Progress In Electromagnetics Research B, Vol. 34, 77–102, 2011

WAVE PROPAGATION IN A HELICAL WAVEGUIDE WITH SLAB AND RECTANGULAR DIELECTRIC PROFILES, AND APPLICATIONS

Z. Menachem* **and S. Tapuchi**

Department of Electrical Engineering, Sami Shamoon College of Engineering, Israel

Abstract—This paper presents a rigorous approach for the propagation of electromagnetic (EM) fields along a helical waveguide with slab and rectangular dielectric profiles in the rectangular cross section. The main objective is to develop a numerical method for the calculation of the output fields, for an arbitrary step's angle and the radius of the cylinder of the helical waveguide. The other objectives are to present the technique to calculate the dielectric profiles and their transverse derivatives in the cross-section and to demonstrate the ability of the model to solve practical problems with slab and rectangular dielectric profiles in the rectangular cross section of the helical waveguide. The method is based on Fourier coefficients of the transverse dielectric profile and those of the input wave profile. Laplace transform is necessary to obtain the comfortable and simple input-output connections of the fields. This model is useful for the analysis of helical waveguides with slab and rectangular dielectric profiles in the metallic helical waveguides in the microwave and the millimeter-wave regimes. The output power transmission and the output power density are improved by increasing the step's angle or the radius of the cylinder of the helical waveguide, especially in the cases of space curved waveguides.

1. INTRODUCTION

Various methods for the analysis of curved waveguides have been studied in the literature. The propagation of general-order modes in curved rectangular waveguide examined by using asymptotic expansion method [1]. A matrix formulation of the generalized telegraphist's

Received 4 July 2011, Accepted 26 August 2011, Scheduled 3 September 2011

* Corresponding author: Zion Menachem (zionm@post.tau.ac.il).

equation [2] used to obtain a general set of equations for a guide of arbitrary cross section with curved axis. The matrix elements involved mode-coupling coefficients which were obtained as rather general integrals of the mode basis functions and the space variables.

Several methods of investigation of propagation were developed for study of empty curved waveguide and bends [3–6]. The results of precise numerical computations and extensive analytical investigation of the angular propagation constants were presented for various electromagnetic modes which may exit in waveguide bends of rectangular cross section [3]. A new equivalent circuit for circular E-plane bends, suitable for any curvature radius and rectangular waveguide type was presented in Ref. [4]. An accurate and efficient method of moments solution together with a mode-matching technique for the analysis of curved bends in a general parallel-plate waveguide was described in the case of a rectangular waveguides [5]. A rigorous differential method describing the propagation of an electromagnetic wave in a bent waveguide was presented in Ref. [6].

Slabs with more general refractive index distributions were considered by Heiblum and Harris [7] and by Kawakami et al. [8], using a WKB method [9]. These two papers consider the case when the mode on the curved waveguide is not a small perturbation of a mode on the straight guide, but was guided essentially by the outer boundary. The modes of this nature are known as "edge-guided" modes. The increase in radiation losses due to curvature for slightly leaky modes on hollow dielectric or imperfect metallic waveguides, a sort of composite of open and closed waveguide behavior, was investigated by Marcatily and Schmeltzer [10].

An analytical method to study a general helix-loaded structure has been published in Ref. [11]. The inhomogeneously-loaded helix enclosed in a cylindrical waveguide operating in the fast-wave regime. The tape-helix model has been used which takes into account the effect of the space-harmonics, and is used particularly in the cases that the structure is operated at high voltages and for high helix pitch angles. The propagation characteristics of an elliptical step-index fiber with a conducting helical winding on the core-cladding boundary [12] are investigated analytically where the coordinate systems are chosen for the circular and elliptical fibers. In their waveguides the core and the cladding regions are assumed to have constant real refractive indices n_1 and n_2, where $n_1 > n_2$. The fibers are referred to as the elliptical helically cladded fiber and the circular helically cladded fiber.

Flow through a helical pipe with rectangular cross-section has been studied in Ref. [13]. The objective was to establish a set of mathematical equations in tensor form that can describe the flow

through a helical duct. Spectral method has been used to solve the non-linear partial differential equations, and the non-linear algebraic equations have been solved by iterative method. A simple field analysis has been developed in Ref. [14] for a helical slow-wave structure symmetrically supported by rectangular shaped discrete dielectric support rods partially embedded in the metal segments projecting radially inward from a metal envelope for wideband traveling-wave tubes. The closed form simplified expressions has been obtained by combining the tape model dispersion relation for free-space helix with the dielectric loading factor obtained for the loaded helix in the sheath model. The analysis of a lossless helical slow-wave structure has been proposed in Ref. [15] for the fundamental mode only, in order to predict the transmission line parameters. The analysis has been developed for the space-harmonic modes considering different radial propagation constant over different structure regions.

An extensive survey of the related literature can be found in the book on electromagnetic waves and curved structures [16]. Propagation in curved rectangular waveguides by the perturbation techniques was introduced for a guide of cross section $a \times b$ whose axis was bent to radius R. Likewise, the twisted coordinate system with application to rectangular waveguides was introduced in Ref. [16]. The other chapters were concerned with curved guides, both rectangular and circular. Calculations were performed for the propagation coefficient, reflection, mode-conversion, mode-coupling and eigenfunctions for a variety of configurations by the asymptotic method. The radiation from curved open structures is mainly considered by using a perturbation approach, that is by treating the curvature as a small perturbation of the straight configuration. The perturbation approach is not entirely suited for the analysis of relatively sharp bends, such as those required in integrated optics and especially short millimeter waves.

An approximate method for predicting the field profile in a curved dielectric waveguide of rectangular cross section was described in [17]. For simplicity, the dielectric and free-space regions were treated separately. Inside the dielectric waveguide, the transverse field was expressed as an Airy function via a conformal transformation. For away from the guide, the field was expressed in terms of Hankel function of the second kind. This model can be applied to guiding structures of rectangular cross section where the transverse propagation constants can be obtained independently.

Several methods of propagation along the toroidal and helical waveguides were developed in [18–23], where the derivation is based on Maxwell's equations. The methods in [18–23] employ toroidal or

helical coordinates (and not cylindrical coordinates, such as in the methods that considered the bending as a perturbation ($r/R \ll 1$)). The method in [18] has been derived for the analysis of EM wave propagation along a toroidal waveguide with a circular dielectric profile in the rectangular cross section. The method in [19] has been derived for the propagation of EM field along a helical waveguide with a circular dielectric profile in the rectangular cross section. The method in [20] has been derived for the propagation of EM field along a toroidal waveguide with a circular dielectric profile in the circular cross section. The method in [21] has been derived for the propagation of EM field along a helical waveguide with a circular dielectric profile in the circular cross section. The method in [22] has been derived for the propagation of EM field along a toroidal waveguide that consists of two bendings with a circular dielectric profile in the circular cross section, and the method for the two bendings was introduced, for small values of step angles (δ_p) of the helical waveguide. The method in [23] has been derived for the propagation of EM field along a helical waveguide that consists of two bendings with a circular dielectric profile in the circular cross section, and the method for the two bendings was introduced, for arbitrary values of step angles.

The main objective of this paper is to develop a theoretical method for the propagation of EM field along the helical waveguide with rectangular dielectric profiles in the rectangular cross section. The other objectives are to present the technique to calculate the dielectric profiles and their transverse derivatives in the cross-section and to demonstrate the ability of the model to solve practical problems with rectangular dielectric profiles in the rectangular cross section of the helical waveguide. This model provides us a numerical tool for the calculation of the output fields and output power transmission for an arbitrary step's angle (δ_p) of the helical waveguide. The method is based on Fourier coefficients of the transverse dielectric profile and those of the input wave profile. This model is useful for the analysis of dielectric waveguides in the microwave and the millimeter-wave regimes. Note that in our method, we do not consider the bending as a perturbation. The purpose of this study was to develop transfer relations between the wave components at the output and input ports of such helical waveguides as matrix functions of their dielectric profiles. The following sections present the derivation of this method for a helical waveguide with slab and rectangular dielectric profiles in the rectangular cross section as function of the step's angle (δ_p) and the radius of the cylinder (R) of the helical waveguide. The output power transmission is improved by increasing the step's angle or the radius of the cylinder of the helical waveguide, especially in the

cases of space curved waveguides.

2. THE DERIVATION

The geometry of the helical waveguide with a rectangular cross section is shown in Fig. 1(a). The direction of the wave propagation is along the axis of the helical waveguide. For small values of the step's angle ($\delta_p \ll 1$), the helical waveguide becomes a toroidal waveguide (Fig. 1(b)), where the radius of the curvature of the helix can then be approximated by the radius of the cylinder.

The axis of the helical waveguide is shown in Fig. 2(a). The deployment of the helix is shown in Fig. 2(b), where R is the radius of the cylinder, and δ_p is the step's angle. We start by finding the metric coefficients from the helical transformation of the coordinates.

The helical transformation of the coordinates is achieved by two rotations and one translation, and is given in the form:

$$\begin{pmatrix} X \\ Y \\ Z \end{pmatrix} = \begin{pmatrix} \cos(\phi_c) & -\sin(\phi_c) & 0 \\ \sin(\phi_c) & \cos(\phi_c) & 0 \\ 0 & 0 & 1 \end{pmatrix} \begin{pmatrix} 1 & 0 & 0 \\ 0 & \cos(\delta_p) & -\sin(\delta_p) \\ 0 & \sin(\delta_p) & \cos(\delta_p) \end{pmatrix} \begin{pmatrix} x \\ 0 \\ y \end{pmatrix}$$

$$+ \begin{pmatrix} R\cos(\phi_c) \\ R\sin(\phi_c) \\ \zeta\sin(\delta_p) \end{pmatrix} = \begin{pmatrix} (R+x)\cos(\phi_c) + y\sin(\delta_p)\sin(\phi_c) \\ (R+x)\sin(\phi_c) - y\sin(\delta_p)\cos(\phi_c) \\ y\cos(\delta_p) + \zeta\sin(\delta_p) \end{pmatrix}, \quad (1)$$

where ζ is the coordinate along the axis of the helical waveguide, R is the radius of the cylinder, δ_p is the step's angle of the helical waveguide (see Figs. 2(a)–2(b)), and $\phi_c = \zeta\cos(\delta_p)/R$. Likewise, $0 \le x \le a$ and

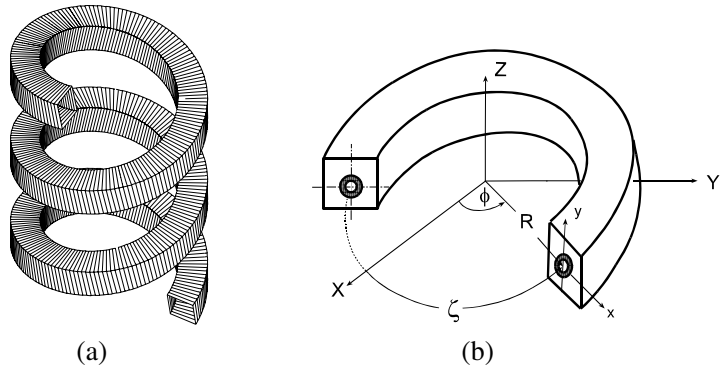

Figure 1. (a) The rectangular helical waveguide. (b) A general scheme of the curved coordinate system (x, y, ζ).

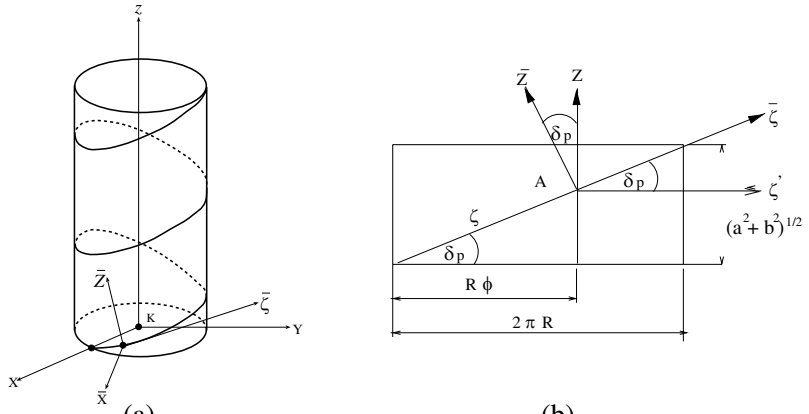

Figure 2. (a) Rotations and translation of the orthogonal system $(\overline{X}, \overline{\zeta}, \overline{Z})$ from point A to the orthogonal system (X, Y, Z) at point K. (b) Deployment of the helix.

$0 \leq y \leq b$, where a and b are the dimensions in the cross section of the helical waveguide. Note that $\zeta \sin(\delta_p) = R\phi_c \tan(\delta_p)$.

Figure 2(a) shows the rotations and translation of the orthogonal system $(\overline{X}, \overline{\zeta}, \overline{Z})$ from point A to the orthogonal system (X, Y, Z) at point K. In the first rotation, the $\overline{\zeta}$ and $\overline{Z}$ axes rotate around the $\overline{X}$ axis of the orthogonal system $(\overline{X}, \overline{\zeta}, \overline{Z})$ at the point A, until the $\overline{Z}$ axis becomes parallel to the Z axis $(\overline{Z} \parallel Z)$, and the $\overline{\zeta}$ axis becomes parallel to the X, Y plane $(\overline{\zeta} \parallel (X, Y))$ of the orthogonal system (X, Y, Z) at the point K. In the second rotation, the $\overline{X}$ and $\overline{\zeta}$ axes rotate around the $\overline{Z}$ axis $(\overline{Z} \parallel Z)$ of the orthogonal system $(\overline{X}, \overline{\zeta}, \overline{Z})$ until $\overline{X} \parallel X$ and $\overline{\zeta} \parallel Y$. After the two above rotations, we have one translation from the orthogonal system $(\overline{X}, \overline{\zeta}, \overline{Z})$ at point A to the orthogonal system (X, Y, Z) at the point K.

Figure 2(b) shows the deployment of the helix depicted in Fig. 2(a). The condition for the step's angle δ_p is given according to

$$\tan(\delta_p) \geq \frac{\sqrt{a^2 + b^2}}{2\pi R}, \tag{2}$$

where the dimensions in the cross section are denoted as a and b, and the radius of the cylinder is denoted as R.

The metric coefficients in the case of the helical waveguide

according to Eq. (1) are:

$$h_x = 1, \tag{3a}$$

$$h_y = 1, \tag{3b}$$

$$\begin{aligned} h_\zeta &= \sqrt{\left(1+\frac{x}{R}\right)^2 \cos^2(\delta_p) + \sin^2(\delta_p)\left(1+\frac{y^2}{R^2}\cos^2(\delta_p)\right)} \\ &= \sqrt{1+\frac{2x}{R}\cos^2(\delta_p) + \frac{x^2}{R^2}\cos^2(\delta_p) + \frac{y^2}{R^2}\cos^2(\delta_p)\sin^2(\delta_p)} \\ &\simeq 1+\frac{x}{R}\cos^2(\delta_p). \end{aligned} \tag{3c}$$

Furthermore, the third and the fourth terms in the root of the metric coefficient h_ζ are negligible in comparison to the first and the second terms when $(x/R)^2 \ll 1$. Nonetheless, the metric coefficient h_ζ still depends on δ_p, the step's angle of the helix (Fig. 2(b)). Note that the metric coefficient h_ζ is a function of x and y, which causes a difficulty in the separation of variables. Thus, the analytical methods are not suitable for the helical or the curved waveguide. The separation of variables is performed in this study, as a numerical method. The case for small values of the step's angle is given in Appendix A.

We assume that for most materials, the permeability μ is equal to that of free space ($\mu = \mu_0$). The wave equations for the electric and magnetic field components in the inhomogeneous dielectric medium $\epsilon(x, y)$ are given by

$$\nabla^2\mathbf{E} + \omega^2\mu\epsilon\mathbf{E} + \nabla\left(\mathbf{E}\cdot\frac{\nabla\epsilon}{\epsilon}\right) = 0, \tag{4a}$$

and

$$\nabla^2\mathbf{H} + \omega^2\mu\epsilon\mathbf{H} + \frac{\nabla\epsilon}{\epsilon}\times(\nabla\times\mathbf{H}) = 0, \tag{4b}$$

respectively. The transverse dielectric profile $\epsilon(x, y)$ is defined as $\epsilon_0(1 + \chi_0 g(x, y))$, where ϵ_0 represents the vacuum dielectric constant, $g(x, y)$ is its profile function in the waveguide, and χ_0 is the susceptibility of the dielectric material. The normalized transverse derivatives of the dielectric profile $g(x, y)$ are defined as $(1/\epsilon(x, y))[(\partial/\partial x)\epsilon(x, y)]$ and $(1/\epsilon(x, y))[(\partial/\partial y)\epsilon(x, y)]$, respectively. From the helical transformation of Eq. (1) we can derive the Laplacian of the vector $\mathbf{E}$ (i.e., $\nabla^2\mathbf{E}$), and obtain the wave equations for the electric and magnetic fields in the inhomogeneous dielectric medium. It is necessary to find the values of $\nabla\cdot\mathbf{E}$, $\nabla(\nabla\cdot\mathbf{E})$, $\nabla\times\mathbf{E}$, and $\nabla\times(\nabla\times\mathbf{E})$ in order to obtain the value of $\nabla^2\mathbf{E}$, where $\nabla^2\mathbf{E} = \nabla(\nabla\cdot\mathbf{E}) - \nabla\times(\nabla\times\mathbf{E})$. All these values are dependent on the metric

coefficients (3a)–(3c). The expressions for $\nabla\cdot\mathbf{E}$, $\nabla\times\mathbf{E}$, and $\nabla\times(\nabla\times\mathbf{E})$ are given in Appendix B.

The components of $\nabla^2\mathbf{E}$ are given by

$$\left(\nabla^2\mathbf{E}\right)_x = \nabla^2 E_x - \frac{1}{R^2h_\zeta^2}\cos^2(\delta_p)E_x - 2\frac{1}{Rh_\zeta^2}\cos^2(\delta_p)\frac{\partial}{\partial\zeta}E_\zeta, \quad (5a)$$

$$\left(\nabla^2\mathbf{E}\right)_y = \nabla^2 E_y, \quad (5b)$$

$$\left(\nabla^2\mathbf{E}\right)_\zeta = \nabla^2 E_\zeta - \frac{1}{R^2h_\zeta^2}\cos^2(\delta_p)E_\zeta + 2\frac{1}{Rh_\zeta^2}\cos^2(\delta_p)\frac{\partial}{\partial\zeta}E_x, \quad (5c)$$

where

$$\nabla^2 = \frac{\partial^2}{\partial x^2} + \frac{\partial^2}{\partial y^2} + \frac{1}{h_\zeta^2}\frac{\partial^2}{\partial\zeta^2} + \frac{1}{Rh_\zeta}\cos^2(\delta_p)\frac{\partial}{\partial x}, \quad (6)$$

and for $h_\zeta = 1 + (x/R)\cos^2(\delta_p)$.

The wave Eqs. (4a) and (4b) are written in the form

$$\left(\nabla^2\mathbf{E}\right)_i + k^2E_i + \partial_i(E_xg_x + E_yg_y) = 0, \quad (7a)$$

$$\left(\nabla^2\mathbf{H}\right)_i + k^2H_i + \partial_i(H_xg_x + H_yg_y) = 0, \quad (7b)$$

where $i = x,\ y,\ \zeta$. The *local* wavenumber parameter is given by $k = \omega\sqrt{\mu\epsilon(x,y)} = k_0\sqrt{1+\chi_0 g(x,y)}$, and the free-space wavenumber is given by $k_0 = \omega\sqrt{\mu_0\epsilon_0}$. The expression $(\nabla^2\mathbf{E})_x$, for instance, is given according to Eq. (5a).

The transverse Laplacian operator is defined as

$$\nabla_\perp^2 = \nabla^2 - \frac{1}{h_\zeta^2}\frac{\partial^2}{\partial\zeta^2}. \quad (8)$$

The metric coefficient h_ζ is a function of x, thus we defined

$$h_\zeta = 1 + p_\zeta(x), \quad p_\zeta(x) = \cos^2(\delta_p)(x/R), \quad (9a)$$

$$h_\zeta^2 = 1 + q_\zeta(x), \quad q_\zeta(x) = \cos^2(\delta_p)(2/R)x. \quad (9b)$$

The Laplace transform

$$\tilde{a}(s) = \mathcal{L}\{a(\zeta)\} = \int_{\zeta=0}^{\infty} a(\zeta)e^{-s\zeta}d\zeta \quad (10)$$

is applied on the ζ-dimension, where $a(\zeta)$ represents any ζ-dependent variables and $\zeta = (R\phi_c)/\cos(\delta_p)$.

Laplace transform on the differential wave equations is needed to obtain the wave equations (and thus also the output fields) that are expressed directly as functions of the transmitted fields at the entrance of the waveguide at $\zeta = 0^+$. Thus, the Laplace transform is necessary

to obtain the comfortable and simple *input-output* connections of the fields.

By substitution of Eqs. (5a)–(5c) into Eqs. (7a) and (7b), by using the Laplace transform (10), and multiply by h_ζ^2, Eqs. (4a) are described in the Laplace transform domain in the form

$$h_\zeta^2\left(\nabla_\perp^2+\frac{s^2}{h_\zeta^2}+k^2\right)\tilde{E}_x+h_\zeta^2\partial_x\left(\tilde{E}_x g_x+\tilde{E}_y g_y\right)+h_\zeta\frac{1}{R}\cos^2(\delta_p)\partial_x\left(\tilde{E}_x\right)$$
$$-\frac{2}{R}\cos^2(\delta_p)s\tilde{E}_\zeta=\left(sE_{x_0}+E_{x_0}^{'}\right)-\frac{2}{R}\cos^2(\delta_p)E_{\zeta_0}, \tag{11}$$

and similarly, the other equations are described in the Laplace transform domain, where the transverse Laplacian operator is defined according to (8), E_{x_0}, $E_{\zeta 0}$ are the initial values of the corresponding fields at $\zeta=0$, i.e., $E_{x_0}=E_x(x,y,\zeta=0)$ and $E_{x_0}^{'}=\frac{\partial}{\partial\zeta}E_x(x,y,\zeta)|_{\zeta=0}$.

The next steps are given in detail in Ref. [19], as a part of our derivation. Let us repeat these steps, in brief.

1). A Fourier transform is applied on the transverse dimension

$$\bar{g}(k_x,k_y)=\mathcal{F}\{g(x,y)\}=\int_x\int_y g(x,y)e^{-jk_x x-jk_y y}dxdy, \tag{12}$$

and the differential equations are transformed to an algebraic form in the (ω,s,k_x,k_y) space.

2). The method of images is applied to satisfy the conditions $\widehat{n}\times E=0$ and $\widehat{n}\cdot(\bigtriangledown\times E)=0$ on the surface of the ideal metallic waveguide walls, where $\widehat{n}$ is a unit vector perpendicular to the surface.

3). The metric coefficient h_ζ is a function of x (Eqs. (9a) and (9b)). Thus the elements of the matrices $\mathbf{P^{(0)}}$ and $\mathbf{Q^{(0)}}$ are defined as:

$$\bar{p_\zeta}^{(o)}_{(n,m)} = \frac{1}{4ab}\int_{-a}^{a}\int_{-b}^{b}p_\zeta(x)\ \ e^{-j(n\frac{\pi}{a}x+m\frac{\pi}{b}y)}\ \ dxdy, \tag{13a}$$

$$\bar{q_\zeta}^{(o)}_{(n,m)} = \frac{1}{4ab}\int_{-a}^{a}\int_{-b}^{b}q_\zeta(x)\ \ e^{-j(n\frac{\pi}{a}x+m\frac{\pi}{b}y)}\ \ dxdy, \tag{13b}$$

and the matrices $\mathbf{P^{(1)}}$ and $\mathbf{Q^{(1)}}$ are defined as:

$$\mathbf{P^{(1)}} = \left(\mathbf{I}+\mathbf{P^{(0)}}\right), \tag{13c}$$

$$\mathbf{Q^{(1)}} = \left(\mathbf{I}+\mathbf{Q^{(0)}}\right), \tag{13d}$$

where $\mathbf{I}$ is the unity matrix.

4). The differential equations are rewritten in a matrix form, where the initial-value vectors, $\hat{E}_{x_0}$, $\hat{E}_{y_0}$, and $\hat{E}_{\zeta_0}$ are defined from the terms $(s\bar{E}_{x_0}+\bar{E}'_{x_0})/2s$, $(s\bar{E}_{y_0}+\bar{E}'_{y_0})/2s$, and $(s\bar{E}_{\zeta_0}+\bar{E}'_{\zeta_0})/2s$, respectively.

The modified wave-number matrices are defined as

$$\begin{aligned}\mathbf{D_x} \equiv\ & \mathbf{K^{(0)}}+\mathbf{Q^{(0)}K1^{(0)}}+\frac{k_o^2\chi_0}{2s}\mathbf{Q^{(1)}G}+\frac{jk_{ox}}{2s}\mathbf{Q^{(1)}NG_x}\\ &+\frac{1}{2sR}\cos^2(\delta_p)jk_{ox}\mathbf{P^{(1)}N}, \qquad (14a)\\ \mathbf{D_y} \equiv\ & \mathbf{K^{(0)}}+\mathbf{Q^{(0)}K1^{(0)}}+\frac{k_o^2\chi_0}{2s}\mathbf{Q^{(1)}G}\\ &+\frac{1}{2sR}\cos^2(\delta_p)jk_{ox}\mathbf{P^{(1)}N}+\frac{jk_{oy}}{2s}\mathbf{Q^{(1)}MG_y}, \qquad (14b)\\ \mathbf{D}_\zeta \equiv\ & \mathbf{K^{(0)}}+\mathbf{Q^{(0)}K1^{(0)}}+\frac{k_o^2\chi_0}{2s}\mathbf{Q^{(1)}G}\\ &+\frac{1}{2sR}\cos^2(\delta_p)jk_{ox}\mathbf{P^{(1)}N}, \qquad (14c)\end{aligned}$$

where the elements of the diagonal matrices $\mathbf{K^{(0)}}$, $\mathbf{M}$, $\mathbf{N}$ and $\mathbf{K^{(1)}}$ are defined as

$$\begin{aligned}K^{(0)}{}_{(n,m)(n',m')} &= \left\{\left[k_o^2-(n\pi/a)^2-(m\pi/b)^2+s^2\right]/2s\right\}\delta_{nn'}\delta_{mm'}, \qquad (15a)\\ M_{(n,m)(n',m')} &= m\delta_{nn'}\delta_{mm'}, \qquad (15b)\\ N_{(n,m)(n',m')} &= n\delta_{nn'}\delta_{mm'}, \qquad (15c)\\ K^{(1)}{}_{(n,m)(n',m')} &= \left\{\left[k_o^2-(n\pi/a)^2-(m\pi/b)^2\right]/2s\right\}\delta_{nn'}\delta_{mm'}, \qquad (15d)\end{aligned}$$

where $\delta_{nn'}$ and $\delta_{mm'}$ are the Kronecker delta functions.

After some algebraic steps, the components of the electric field are formulated as follows:

$$\begin{aligned}E_x = &\left\{\mathbf{D_x}+\alpha_1\mathbf{Q^{(1)}M_1Q^{(1)}M_2}+\frac{1}{R}\cos^2(\delta_p)\mathbf{D}_\zeta{}^{-1}\right.\\ &\left.\left(-\frac{1}{2}\mathbf{Q^{(1)}G_x}+\frac{1}{2}\alpha_2\mathbf{Q^{(1)}M_3Q^{(1)}M_2}-\frac{1}{R}\cos^2(\delta_p)\mathbf{I}\right)\right\}^{-1}\\ &\left(\hat{E}_{x_0}-\frac{1}{sR}\cos^2(\delta_p)E_{\zeta_0}-\alpha_3\mathbf{Q^{(1)}M_1}\hat{E}_{y_0}+\frac{1}{R}\cos^2(\delta_p)\mathbf{D}_\zeta{}^{-1}\right.\\ &\left.\left(\hat{E}_{\zeta_0}+\frac{1}{sR}\cos^2(\delta_p)E_{x_0}+\frac{1}{2s}\mathbf{Q^{(1)}}(\mathbf{G_x}E_{x_0}+\mathbf{G_y}E_{y_0})-\frac{1}{2}\mathbf{Q^{(1)}M_3}\hat{E}_{y_0}\right)\right), \qquad (16a)\end{aligned}$$

$$E_y = \mathbf{D_y}^{-1}\left(\hat{E}_{y_0} - \frac{jk_{oy}}{2s}\mathbf{Q^{(1)}}\mathbf{M}\mathbf{G_x}E_x\right), \tag{16b}$$

$$E_\zeta = \mathbf{D}_\zeta{}^{-1}\left\{\hat{E}_{\zeta_0} + \frac{1}{2s}\mathbf{Q^{(1)}}\left(\mathbf{G_x}E_{x_0} + \mathbf{G_y}E_{y_0}\right)\right.$$
$$\left. -\frac{1}{2}\mathbf{Q^{(1)}}\left(\mathbf{G_x}E_x + \mathbf{G_y}E_y\right) - \frac{1}{R}\cos^2(\delta_p)E_x + \frac{1}{sR}\cos^2(\delta_p)E_{x_0}\right\}, \tag{16c}$$

where: $\alpha_1 = \frac{k_{ox}k_{oy}}{4s^2}$, $\alpha_2 = \frac{jk_{oy}}{2s}$, $\alpha_3 = \frac{jk_{ox}}{2s}$, $\mathbf{M_1} = \mathbf{N}\mathbf{G_y}\mathbf{D_y}^{-1}$, $\mathbf{M_2} = \mathbf{M}\mathbf{G_x}$, $\mathbf{M_3} = \mathbf{G_y}\mathbf{D_y}^{-1}$.

These equations describe the transfer relations between the spatial spectrum components of the output and input waves in the dielectric waveguide. Similarly, the other components of the magnetic field are obtained. The transverse field profiles are computed by the inverse Laplace and Fourier transforms, as follows

$$E_y(x, y, \zeta) = \sum_n \sum_m \int_{\sigma - j_\infty}^{\sigma + j_\infty} E_y(n, m, s) e^{jnk_{ox}x + jmk_{oy}y + s\zeta} ds. \tag{17}$$

The inverse Laplace transform is performed in this study by a direct numerical integration on the s-plane by the method of Gaussian Quadrature. The integration path in the right side of the s-plane includes all the singularities, as proposed by Salzer [24, 25].

The ζ component of the average-power density of the complex Poynting vector is given by

$$S_{av} = \frac{1}{2}\mathrm{Re}\left\{E_x {H_y}^* - E_y {H_x}^*\right\}, \tag{18}$$

where the asterisk indicates the complex conjugate. The active power is equal to the real part of the complex Poynting vector. The total average-power transmitted along the guide in the ζ direction is given by a double integral of Eq. (18). A Fortran code is developed using NAG subroutines [26]. Several examples computed on a Unix system are presented in the next section.

3. NUMERICAL RESULTS

This section presents several examples which demonstrate features of the proposed mode model derived in the previous section. The method of this model is based on Fourier coefficients, thus the accuracy of the method is dependent on the number of the modes in the system.

Further we assume $N = M$. The convergence of the solution is verified by the criterion

$$C(N) \equiv \log\left\{ \frac{\max\left(\left|S_{av}^{N+2} - S_{av}^{N}\right|\right)}{\left|\max\left(S_{av}^{N+2}\right) - \min\left(S_{av}^{N}\right)\right|} \right\}, \qquad N \geq 1, \tag{19}$$

where the number of the modes is equal to $(2N+1)^2$. The order N determines the accuracy of the solution. If the value of the criterion is less then -2, then the numerical solution is well converged.

A comparison with the known transcendental equation [27] is needed, in order to examine the validity of the theoretical model. We derive the transcendental equation and the field E_y by the potentials for TE_{10} mode. We confirm the validity of our model by comparison of the numerically computed results with the results based on the transcendental equation for a dielectric slab (Fig. 3).

Let us compare the theoretical model with the known analytical theory. For the given dimensions a and d, we find the values Λ and Ω according to the next transcendental equation for a dielectric slab (Fig. 3). According to our theoretical model we can calculate $E_{y_0}(n,m)$ and $g(n,m)$ as follows:

$$E_{y_0}(n,m) = \frac{1}{4ab}\int_{-a}^{a}\int_{-b}^{b} E_y(x,y,z=0)e^{-j(n\frac{\pi}{a}x + m\frac{\pi}{b}y)}dxdy,$$

and

$$g(n,m) = \frac{1}{4ab}\int_{-a}^{a}\int_{-b}^{b} g(x,y)e^{-j(n\frac{\pi}{a}x + m\frac{\pi}{b}y)}dxdy.$$

The derivation of the transcendental equation [27] is given as follows.

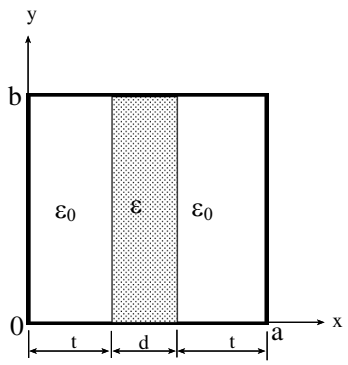

Figure 3. A dielectric slab in a rectangular metallic waveguide.

The potentials for TE_{10} mode (Fig. 3) are given according to

$$\begin{cases} \Psi_1 = C_1 \sin(k_{x1}x)e^{-jk_z z} \\ \Psi_2 = \left[C_{21}\sin(k_{x2}(x-(\frac{a}{2})) + C_{22}\cos(k_{x2}(x-(\frac{a}{2}))\right] e^{-jk_z z} \\ \Psi_3 = C_3 \sin(k_{x3}(a-x))e^{-jk_z z} \end{cases},$$

where k_z is the propagation constant. The Dispersion-Equations

$$\begin{cases} k_{x1}^2 + k_z^2 = \omega^2\mu_0\epsilon_0 = k_o^2 \\ k_{x3}^2 + k_z^2 = \omega^2\mu_0\epsilon_0 = k_o^2 \\ k_{x2}^2 + k_z^2 = \omega^2\mu_0\epsilon = k_o^2\epsilon_r \end{cases},$$

where $k_{x1} = k_{x3}$.

From the symmetric solutions ($C_1 = C_3,\ C_{21} = 0$) for E_y and H_z we obtain

$$E_y = -\frac{1}{\epsilon}\frac{\partial\psi}{\partial z} = jk_z\frac{1}{\epsilon}\psi, \qquad H_z = \frac{1}{j\omega\mu\epsilon}\frac{\partial^2\psi}{\partial x\partial z} = -\frac{k_z}{\omega\mu\epsilon}\frac{\partial\psi}{\partial x}.$$

By the continuity request in the regions $x = t$ and $x = a-t$ (see Fig. 3) for E_y and H_z, and by division of the equations, one can obtain for the symmetric case the transcendental equation

$$\nu\cot(\nu t) = \mu\tan(\mu d/2),$$

where $\nu \equiv \sqrt{k_o^2 - k_z^2}$, $\mu \equiv \sqrt{k_o^2\epsilon_r - k_z^2}$ and $(a-2t)/2 = d/2$.

For the symmetric solution ($C_1 = C_3,\ C_{21} = 0$) we obtain

$$\begin{cases} E_{y1} = j\frac{k_z}{\epsilon_0}\sin(\nu x)e^{-jk_z z} & 0 < x < t \\ E_{y2} = j\frac{k_z}{\epsilon_0}\frac{\sin(\nu\cdot t)}{\cos(\mu(t-a/2))}\cos\left[\mu(x-\frac{a}{2})\right]e^{-jk_z z} & t < x < t+d \\ E_{y3} = j\frac{k_z}{\epsilon_0}\sin\left[\nu(a-x)\right]e^{-jk_z z} & t+d < x < a \end{cases}.$$

The solution for the dielectric slab modes based on transcendental equation [27] is given as follows

$$\begin{cases} E_{y1} = j\frac{k_z}{\epsilon_0}\sin(\nu x) & 0 < x < t \\ E_{y2} = j\frac{k_z}{\epsilon_0}\frac{\sin(\nu t)}{\cos(\mu(t-a/2))}\cos\left[\mu(x-a/2)\right] & t < x < t+d \\ E_{y3} = j\frac{k_z}{\epsilon_0}\sin\left[\nu(a-x)\right] & t+d < x < a \end{cases}, \quad (20)$$

where $\nu \equiv \sqrt{k_o^2 - k_z^2}$ and $\mu \equiv \sqrt{\epsilon_r k_o^2 - k_z^2}$ result from the transcendental equation

$$\left(\frac{a}{d} - 1\right)\frac{d\mu}{2}\tan\left(\frac{d\mu}{2}\right) - (t\nu)\cot(t\nu) = 0,$$

and

$$\frac{\partial}{\partial z}E_y(x,y,z)|_{z=0} = -jk_z E_y(x,y,z=0).$$

Let us denote $\Lambda \equiv (d/2)\mu$ and $\Omega \equiv t\nu$. For the given dimensions a and d, we find the values Λ and Ω according to the next transcendental equation

$$\left(\frac{a}{d} - 1\right)\Lambda \tan \Lambda - \Omega \cot \Omega = 0,$$

where $\Omega \neq k\pi$ and $\Lambda \neq (2k+1)(\pi/2)$.

By addition and subtraction of the equations $\nu^2 = k_o^2 - k_z^2$ and $\mu^2 = \epsilon_r k_o^2 - k_z^2$ we obtain

$$k_o = \left(\frac{(2\Lambda/d)^2 - (\Omega/t)^2}{\epsilon_r - 1}\right)^{1/2}, \qquad k_z = \left(\frac{(2\Lambda/d)^2 - \epsilon_r\,(\Omega/t)^2}{\epsilon_r - 1}\right)^{1/2}.$$

Equation (20) were substituted as the initial fields into the Eq. (16(b)) at $z = 0^+$ in the practical case of the straight waveguide (by letting $R \to \infty$ or by taking $\delta_p = \pi/2$) with the symmetrical slab profile (Fig. 3). The result of the comparison between the theoretical model with the known solution [27] is shown in Fig. 4(a), where $\epsilon_r = 9$, $d = 3.3\,\text{mm}$, and $\lambda = 6.9\,\text{cm}$. The convergence of the numerical results as a function of the matrix order is shown in Fig. 4(b). The comparison is demonstrated for every order ($N = 1$, 3, 5, 7, and 9). The order N determines the accuracy of the solution. The convergence of the

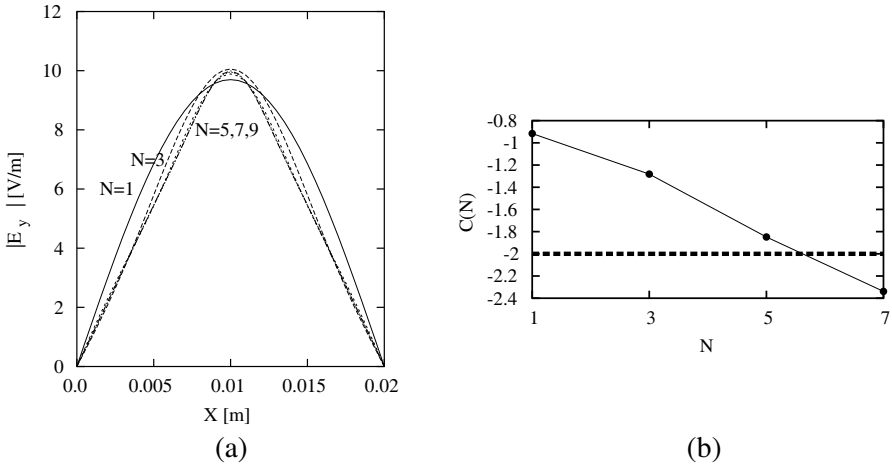

Figure 4. (a) A comparison between amplitude results of the theoretical model and the transcendental equation ($a = 2b = 2\,\text{cm}$, $d = 3.3\,\text{mm}$, $\epsilon_r = 9$, and $\lambda = 6.9\,\text{cm}$; (b). The convergence of our theoretical results.

solution is verified by the criterion (19) for the E_y component of the fields (instead of S_{av}). If the value of the criterion is less then -2, then the numerical solution is well converged. When N increases, then $E_y(N)$ approaches E_y. The value of the criterion between $N = 7$ and $N = 9$ is equal to $-2.38 \simeq -2$, namely a hundredth part. The comparison between the theoretical mode-model and the known model [27] has shown good agreement.

Note that we have two ways to compare between the results of our mode model with the other methods. The first way is to compare between the results of the output fields for every order ($N = 1$, 3, 5, 7, and 9) with the final solution of the known method. The second way is to compare between the results of the output fields (according to our model) for every two orders ($N = 1$, 3, $N = 3$, 5, $N = 5$, 7, and $N = 7$, 9), until our numerical solution is well converged. This way is efficient in the cases that we have complicated problems that we cannot compare with the final solution of the known method.

3.1. A Rectangular Dielectric Profile in the Rectangular Cross Section of the Metallic Helical Waveguide

The geometrical shape of a rectangular dielectric profile loaded in the rectangular cross section of the metallic helical waveguide is demonstrated in Fig. 5 for an inhomogeneous dielectric profile in the cross section. The dimensions of the waveguide in the cross-section are denoted as a and b. Further, the next examples will demonstrate the results of the solutions in the case of a rectangular dielectric profile loaded in the rectangular cross section of the metallic helical waveguide (Fig. 5), for $a = b = 2\,\text{cm}$.

In order to solve discontinuous problems in the cross section, the

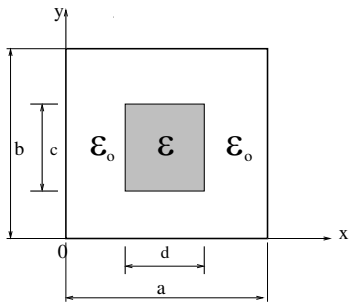

Figure 5. A rectangular dielectric profile loaded in the rectangular cross section of the metallic helical waveguide.

ω_ε function, "cap-shaped function" [28], is used. The ω_ε function (Fig. 6(a)) is defined as

$$\omega_\varepsilon(r) = \begin{cases} C_\varepsilon e^{-\frac{\varepsilon^2}{\varepsilon^2 - |r|^2}} & |r| \le \varepsilon \\ 0 & |r| > \varepsilon \end{cases},$$

where the constant C_ε is chosen to satisfy $\int \omega_\varepsilon(r)dr = 1$.

The ω_ε function in the limit $\varepsilon \longrightarrow 0$ is shown in Fig. 6(b). The dielectric profile $g(x)$ and $g(y)$ in this case of a rectangular dielectric profile in the rectangular cross section (Fig. 5) are given by

$$g(x) = \begin{cases} 0 & 0 \le x < (a-d-\varepsilon_1)/2 \\ g_0 \exp\left[1 - \frac{{\varepsilon_1}^2}{{\varepsilon_1}^2 - [x-(a-d+\varepsilon_1)/2)]^2}\right] & (a-d-\varepsilon_1)/2 \le x < (a-d+\varepsilon_1)/2 \\ g_0 & (a-d+\varepsilon_1)/2 < x < (a+d-\varepsilon_2)/2, \\ g_0 \exp\left[1 - \frac{{\varepsilon_2}^2}{{\varepsilon_2}^2 - [x-(a+d-\varepsilon_2)/2)]^2}\right] & (a+d-\varepsilon_2)/2 \le x < (a+d+\varepsilon_2)/2 \\ 0 & (a+d+\varepsilon_2)/2 < x \le a \end{cases}$$

$$g(y) = \begin{cases} 0 & 0 \le y < (b-c-\varepsilon_1)/2 \\ g_0 \exp\left[1 - \frac{{\varepsilon_1}^2}{{\varepsilon_1}^2 - [y-(b-c+\varepsilon_1)/2)]^2}\right] & (b-c-\varepsilon_1)/2 \le y < (b-c+\varepsilon_1)/2 \\ g_0 & (b-c+\varepsilon_1)/2 < y < (b+c-\varepsilon_2)/2. \\ g_0 \exp\left[1 - \frac{{\varepsilon_2}^2}{{\varepsilon_2}^2 - [y-(b+c-\varepsilon_2)/2)]^2}\right] & (b+c-\varepsilon_2)/2 \le y < (b+c+\varepsilon_2)/2 \\ 0 & (b+c+\varepsilon_2)/2 < y \le a \end{cases}$$

The elements of the matrice $g(n, m)$ are given according to Fig. 5, in

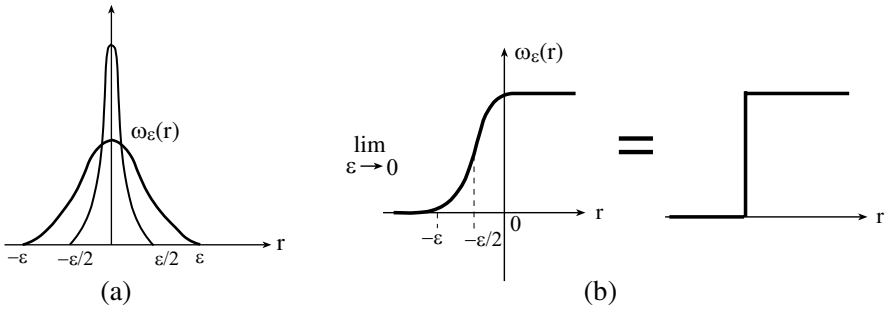

Figure 6. (a) The ω_ε function. (b) The ω_ε function in the limit $\varepsilon \longrightarrow 0$.

the case of $b \neq c$ by

$$
\begin{aligned}
&g(n,m) = \\
&\frac{g_0}{ab}\left\{\int_{(a-d-\varepsilon_1)/2}^{(a-d+\varepsilon_1)/2} \exp\left[1-\frac{{\varepsilon_1}^2}{{\varepsilon_1}^2-[x-(a-d+\varepsilon_1)/2)]^2}\right]\cos\left(\frac{n\pi x}{a}\right)dx\right. \\
&+\int_{(a-d-\varepsilon_1)/2}^{(a+d-\varepsilon_2)/2}\cos\left(\frac{n\pi x}{a}\right)dx \\
&\left.+\int_{(a+d-\varepsilon_2)/2}^{(a+d+\varepsilon_2)/2}\exp\left[1-\frac{{\varepsilon_1}^2}{{\varepsilon_1}^2-[x-(a+d-\varepsilon_2)/2)]^2}\right]\cos\left(\frac{n\pi x}{a}\right)dx\right\} \\
&\left\{\int_{(b-c-\varepsilon_1)/2}^{(b-c+\varepsilon_1)/2}\exp\left[1-\frac{{\varepsilon_1}^2}{{\varepsilon_1}^2-[y-(b-c+\varepsilon_1)/2)]^2}\right]\cos\left(\frac{m\pi y}{b}\right)dy\right. \\
&+\int_{(b-c-\varepsilon_1)/2}^{(b+c-\varepsilon_2)/2}\cos\left(\frac{m\pi y}{b}\right)dy \\
&\left.+\int_{(b+c-\varepsilon_2)/2}^{(b+c+\varepsilon_2)/2}\exp\left[1-\frac{{\varepsilon_1}^2}{{\varepsilon_1}^2-[y-(b+c-\varepsilon_2)/2)]^2}\right]\cos\left(\frac{m\pi y}{b}\right)dy\right\}.
\end{aligned}
$$

The elements of the matrice $g(n,m)$ are given according to Fig. 5, in the case of $b = c$ by

$$
\begin{aligned}
&g(n,m) = \\
&\frac{g_0}{ab}\left\{\int_{(a-d-\varepsilon_1)/2}^{(a-d+\varepsilon_1)/2}\exp\left[1-\frac{{\varepsilon_1}^2}{{\varepsilon_1}^2-[x-(a-d+\varepsilon_1)/2)]^2}\right]\cos\left(\frac{n\pi x}{a}\right)dx\right. \\
&+\int_{(a-d-\varepsilon_1)/2}^{(a+d-\varepsilon_2)/2}\cos\left(\frac{n\pi x}{a}\right)dx \\
&\left.+\int_{(a+d-\varepsilon_2)/2}^{(a+d+\varepsilon_2)/2}\exp\left[1-\frac{{\varepsilon_1}^2}{{\varepsilon_1}^2-[x-(a+d-\varepsilon_2)/2)]^2}\right]\cos\left(\frac{n\pi x}{a}\right)dx\right\} \\
&\left\{\int_0^b\cos\left(\frac{m\pi y}{b}\right)dy\right\}.
\end{aligned}
$$

The derivatives of the dielectric profile are defined as

$$
\begin{aligned}
g_x &\equiv \frac{1}{\epsilon(x,y)}\frac{\partial\epsilon(x,y)}{\partial x} = \frac{\partial[\ln(1+g(x,y))]}{\partial x}, \\
g_y &\equiv \frac{1}{\epsilon(x,y)}\frac{\partial\epsilon(x,y)}{\partial y} = \frac{\partial[\ln(1+g(x,y))]}{\partial y}.
\end{aligned}
$$

Thus, the derivatives of the dielectric profile are calculated as follow

$$g_x = \begin{cases} 0 & 0 \le x < (a-d-\varepsilon_1)/2 \\ \frac{d}{dx}\left\{ln\left[1+g_0\exp\left[1-\frac{{\varepsilon_1}^2}{{\varepsilon_1}^2-[x-(a-d+\varepsilon_1)/2)]^2}\right]\right]\right\} & (a-d-\varepsilon_1)/2 \le x < (a-d+\varepsilon_1)/2 \\ 0 & (a-d+\varepsilon_1)/2 < x < (a+d-\varepsilon_2)/2 \\ \frac{d}{dx}\left\{ln\left[1+g_0\exp\left[1-\frac{{\varepsilon_2}^2}{{\varepsilon_2}^2-[x-(a+d-\varepsilon_2)/2)]^2}\right]\right]\right\} & (a+d-\varepsilon_2)/2 \le x < (a+d+\varepsilon_2)/2 \\ 0 & (a+d+\varepsilon_2)/2 < x \le a \end{cases},$$

$$g_y = \begin{cases} 0 & 0 \le y < (b-c-\varepsilon_1)/2 \\ \frac{d}{dx}\left\{ln\left[1+g_0\exp\left[1-\frac{{\varepsilon_1}^2}{{\varepsilon_1}^2-[y-(b-c+\varepsilon_1)/2)]^2}\right]\right]\right\} & (b-c-\varepsilon_1)/2 \le y < (b-c+\varepsilon_1)/2 \\ 0 & (b-c+\varepsilon_1)/2 < y < (b+c-\varepsilon_2)/2 \\ \frac{d}{dx}\left\{ln\left[1+g_0\exp\left[1-\frac{{\varepsilon_2}^2}{{\varepsilon_2}^2-[y-(b+c-\varepsilon_2)/2)]^2}\right]\right]\right\} & (b+c-\varepsilon_2)/2 \le x < (a+d+\varepsilon_2)/2 \\ 0 & (b+c+\varepsilon_2)/2 < y \le b \end{cases}.$$

The main contribution of this paper is demonstrated in Fig. 7, in order to understand the influence of the step's angle (δ_p) and the radius of the cylinder (R) on the output power transmission. The output fields are dependent on the input wave profile (TE_{10} mode) and the dielectric profile. Six results are demonstrated for six values of δ_p ($\delta_p = 0,\ 0.4,\ 0.7,\ 0.8,\ 0.9,\ 1.0$), where $\zeta = 15\,\text{cm}$, $a = 2\,\text{cm}$, $b = c = 2\,\text{cm}$, $d = 1.6\,\text{cm}$, $\lambda = 3.75\,\text{cm}$, and $\epsilon_r = 1.5$, in the practical case of the slab dielectric profile (Fig. 5). For an arbitrary value of R, the output power transmission is large for large values of δ_p and decreases with decreasing the value of δ_p. On the other hand, for an arbitrary value of δ_p, the output power transmission is large for large values of R and decreases with decreasing the value of R. Note that for small values of the step's angle, the radius of curvature of the helical waveguide can be approximated by the radius of the cylinder. In this case, the output power transmission is large for small values of the bending ($1/R$), and decreases with increasing the bending. Thus, this model can be a useful tool to find the parameters (δ_p and R) which will give us the improved results (output power transmission) of the curved waveguide in the cases of space curved waveguides.

Figures 8(a)–(b) show the results of the output power density (S_{av}) as function of ϵ_r in the case of the slab dielectric profile ($a = 20\,\text{mm}$,

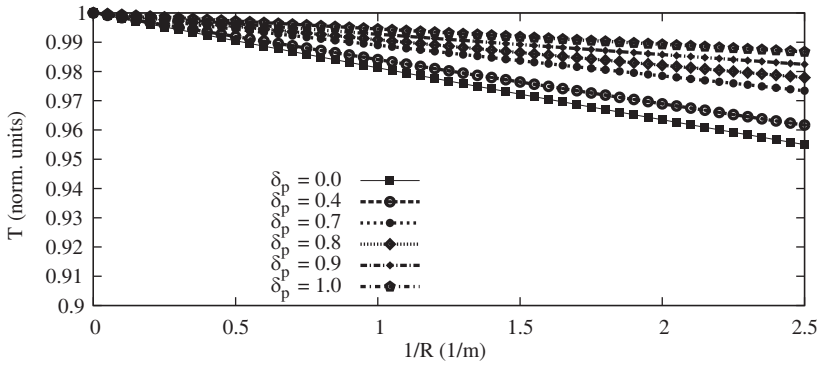

Figure 7. The results of the output power transmission as a function of $1/R$, where R is the radius of the cylinder. Six results are demonstrated for six values of δ_p (δ_p = 0.0, 0.4, 0.7, 0.8, 0.9, 1.0), where $\zeta = 15\,\text{cm}$, $a = 20\,\text{mm}$, $b = c = 20\,\text{mm}$, $d = 16\,\text{mm}$, $\lambda = 3.75\,\text{cm}$, and $\epsilon_r = 1.5$.

$b = c = 20\,\text{mm}$, and $d = 16\,\text{mm}$), where $\epsilon_r = 1.5$, 2.0, respectively. Figs. 8(c)–(f) show the results of the output power density (S_{av}) as function of ϵ_r in the case of the rectangular dielectric profile in the rectangular cross section ($a = b = 20\,\text{mm}$, and $c = d = 16\,\text{mm}$), where $\epsilon_r = 1.5$, 1.6, 1.75, and 2.0, respectively. The other parameters are given for the step's angle ($\delta_p = 1$) and the radius of the cylinder ($R = 0.26\,\text{m}$), where $\zeta = 15\,\text{cm}$, and $\lambda = 3.75\,\text{cm}$. The output fields are dependent on the input wave profile (TE_{10} mode) and the dielectric profile (Fig. 5).

Figure 9(a) shows the output amplitude and the output profile shape for four values of $\epsilon_r = 1.5$, 1.6, 1.75, and 2.0, respectively. The output profile is shown in the same cross section of output transverse profile of Fig. 8(a), where $y = b/2 = 10\,\text{mm}$. By changing only the value of the parameter ϵ_r of the slab dielectric profile from 1.5 to 2.0, the output transverse profile of the power density (S_{av}) is changed, and the amplitude of the output power density is changed from $1\,\text{W/m}^2$ to $0.5\,\text{W/m}^2$, as shown in Figs. 8(a)–(b). By changing only the value of the parameter ϵ_r of the rectangular dielectric profile in the rectangular cross section (Fig. 5) from 1.5 to 2.0, the output transverse profile of the power density (S_{av}) is changed, and the amplitude of the output power density is changed from $1.6\,\text{W/m}^2$ to $0.9\,\text{W/m}^2$, as shown in Figs. 8(c)–(f). The amplitude of the output power density decreases with increasing the value of ϵ_r. These examples demonstrate the influence of the slab and rectangular dielectric profiles in the rectangular cross section of the helical waveguide, for arbitrary step's angle and the radius of the cylinder of the helical waveguide.

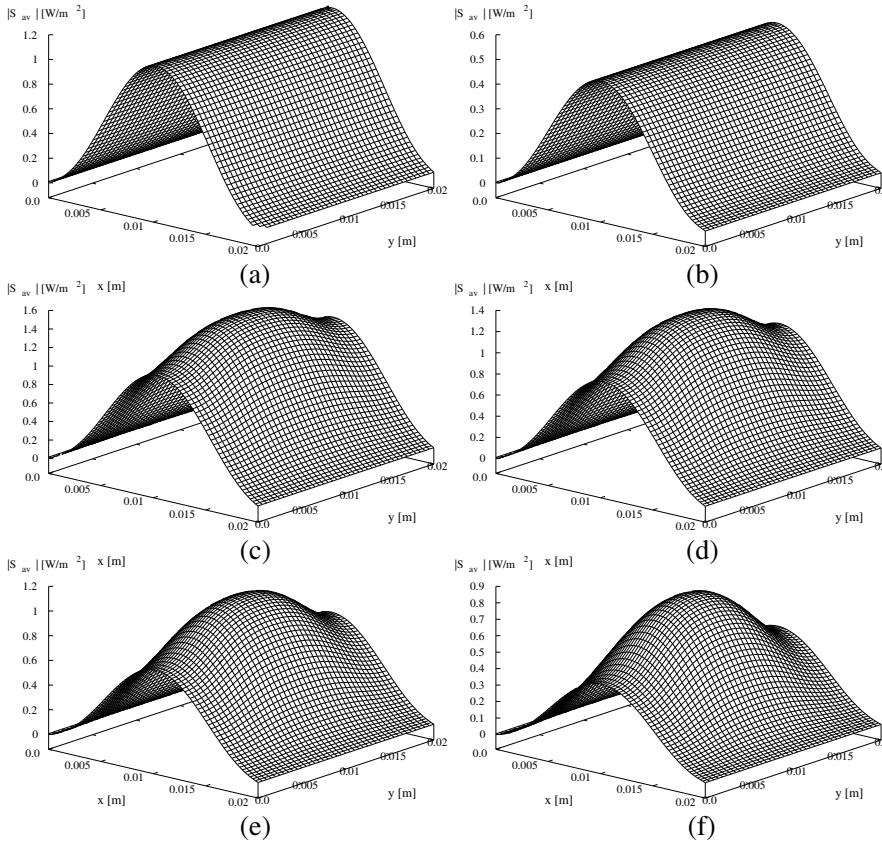

Figure 8. The results of the output power density as function of ϵ_r in the case of the slab dielectric profile ($a = 20\,\text{mm}$, $b = c = 20\,\text{mm}$, and $d = 16\,\text{mm}$). (a). $\epsilon_r = 1.5$; (b) $\epsilon_r = 2.0$. The results of the rectangular dielectric profile in the rectangular cross section ($a = b = 20\,\text{mm}$, and $c = d = 16\,\text{mm}$). (c) $\epsilon_r = 1.5$; (d) $\epsilon_r = 1.6$; (e) $\epsilon_r = 1.75$; (f) $\epsilon_r = 2.0$. The other parameters are $\lambda = 3.75\,\text{cm}$, $\delta_p = 1$, $R = 0.26\,\text{m}$, and $\zeta = 15\,\text{cm}$.

Figure 9(b) shows an example for the output profiles for $N = 1$, 3, 5 and 7, where $\epsilon_r = 1.5$. The output results are demonstrated for every order ($N = 1$, 3, 5, and 7). By increasing only the parameter of the order from $N = 1$ to $N = 7$, then the output profile approaches to the final output profile.

It is very interesting to understand the behaviour of the results that are demonstrated in Figs. 7, 8(a)–(f), and 9(a)–(b) in the case of a helical waveguide with slab and rectangular dielectric profiles with the

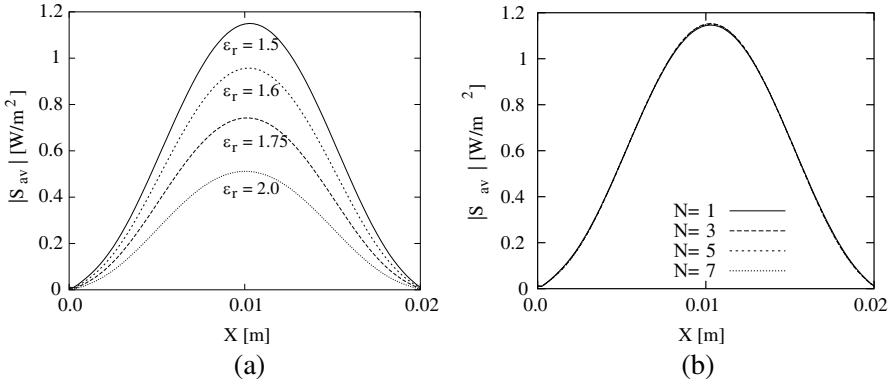

Figure 9. (a) The output amplitude and the profile shape of the central peak in the same cross section of Fig. 8(a) where $y = b/2 = 10\,\text{mm}$, in the case of the slab dielectric profile ($a = 20\,\text{mm}$, $b = c = 20\,\text{mm}$, and $d = 16\,\text{mm}$). The output modal profile is given for the step's angle ($\delta_p = 1$) and the radius of the cylinder ($R = 0.26\,\text{m}$), where $\zeta = 15\,\text{cm}$, $\lambda = 3.75\,\text{cm}$, and for different values of ϵ_r. (b) The output profile for $N = 1$, 3, 5, and 7, where $\epsilon_r = 1.5$.

results in Ref. [19] in the case of a helical waveguide with the circular dielectric profile. We can't compare between the different methods, but the behaviour of the results in Fig. 7 and in Ref. [19] shows that for an arbitrary value of R, the output power transmission is large for large values of δ_p and decreases with decreasing the value of δ_p. On the other hand, for an arbitrary value of δ_p, the output power transmission is large for large values of R and decreases with decreasing the value of R. Thus, this model and the model in Ref. [19] can be a useful tool to find the parameters (δ_p and R) which will give us the improved results (output power transmission) of the curved waveguide in the cases of space curved waveguides.

The influence of the parameter ϵ_r on the profiles and the amplitude of the output power density (S_{av}) is demonstrated in Figs. 8(a)–(f), and 9(a)–(b) and in Ref. [19] in the different cases. The examples in Figs. 8(a)–(f) and 9(a)–(b) are demonstrated in the cases of a helical waveguide with slab and rectangular dielectric profiles and the examples in Ref. [19] are demonstrated in the case of a helical waveguide with the circular dielectric profile. In spite of the differences, the two methods refer to the propagation of EM fields along a helical waveguide, for an arbitrary step's angle (δ_p) and the radius of the cylinder (R) in practical cases of the dielectric profiles in the rectangular cross section.

4. CONCLUSION

This paper presents a rigorous approach for the propagation of EM fields along a helical waveguide with slab and rectangular dielectric profiles in the rectangular cross section. The main objective was to develop a numerical method for the calculation of the output fields, for an arbitrary step's angle (δ_p) and the radius of the cylinder of the helical waveguide. This method was developed for a helical waveguide (a space curved waveguide for an arbitrary value of the step's angle of the helical waveguide) with slab and rectangular dielectric profiles in the rectangular cross section. The other objectives were to present the technique to calculate the dielectric profiles and their transverse derivatives in the cross-section and to demonstrate the ability of the model to solve practical problems with slab and rectangular dielectric profiles. These slab and rectangular dielectric profiles in the rectangular cross section of the helical waveguide are examples to practical problems with inhomogeneous dielectric profiles, in the microwave and the millimeter-wave regimes.

The calculations are based on using Laplace and Fourier transforms, and the output fields are computed by the inverse Laplace and Fourier transforms. Laplace transform on the differential wave equations is needed to obtain the wave equations (and thus also the output fields) that are expressed directly as functions of the transmitted fields at the entrance of the waveguide at $\zeta = 0^+$. Thus, the Laplace transform is necessary to obtain the comfortable and simple *input-output* connections of the fields. The output fields are dependent on the input wave profile (TE_{10} mode) and the dielectric profile.

The main contribution of this paper is demonstrated in Fig. 7, in order to understand the influence of the step's angle (δ_p) and the radius of the cylinder (R) on the output power transmission. Six results are demonstrated for six values of δ_p (δ_p =0, 0.4, 0.7, 0.8, 0.9, 1.0), where $\zeta = 15\,\text{cm}$, $a = 2\,\text{cm}$, $b = c = 2\,\text{cm}$, $d = 1.6\,\text{cm}$, $\lambda = 3.75\,\text{cm}$, and $\epsilon_r = 1.5$, in the practical case of the slab dielectric profile (Fig. 5). For an arbitrary value of R, the output power transmission is large for large values of δ_p and decreases with decreasing the value of δ_p. On the other hand, for an arbitrary value of δ_p, the output power transmission is large for large values of R and decreases with decreasing the value of R. Note that for small values of the step's angle, the radius of curvature of the helical waveguide can be approximated by the radius of the cylinder. In this case, the output power transmission is large for small values of the bending ($1/R$), and decreases with increasing the bending. Thus, this model can be a useful tool to find the parameters (δ_p and R)

which will give us the improved results (output power transmission) of the curved waveguide in the cases of space curved waveguides.

Figures 8(a)–(b) show the results of the output power density (S_{av}) as function of ϵ_r in the case of the slab dielectric profile ($a = 20\,\text{mm}$, $b = c = 20\,\text{mm}$, and $d = 16\,\text{mm}$), where $\epsilon_r = 1.5$, 2.0, respectively. Figs. 8(c)–(f) show the results of the output power density (S_{av}) as function of ϵ_r in the case of the rectangular dielectric profile in the rectangular cross section ($a = b = 20\,\text{mm}$, and $c = d = 16\,\text{mm}$), where $\epsilon_r = 1.5$, 1.6, 1.75, and 2.0 respectively. The other parameters are given for the step's angle ($\delta_p = 1$) and the radius of the cylinder ($R = 0.26\,\text{m}$), where $\zeta = 15\,\text{cm}$, and $\lambda = 3.75\,\text{cm}$.

Figure 9(a) shows the output amplitude and the output profile shape for four values of $\epsilon_r = 1.5$, 1.6, 1.75, and 2.0, respectively. The amplitude of the output power density decreases with increasing the value of the parameter ϵ_r in the slab and rectangular dielectric profiles, and the output transverse profile of the power density (S_{av}) is changed, as shown in Figs. 8(a)–(f) and Fig. 9(a).

Figure 9(b) shows an example for the output profiles for $N = 1$, 3, 5, and 7, where $\epsilon_r = 1.5$. The output results are demonstrated for every order ($N = 1$, 3, 5, and 7). By increasing only the parameter of the order from $N = 1$ to $N = 7$, then the output profile approaches to the final output profile.

These examples demonstrate the influence of the slab and rectangular dielectric profiles in the rectangular cross section of the helical waveguide, for arbitrary step's angle and the radius of the cylinder of the helical waveguide. This model is useful for the analysis of helical waveguides with rectangular dielectric profiles in the microwave and the millimeter-wave regimes. This model can be a useful tool to find the parameters (δ_p and R) which will give us the improved results (output power transmission) of the curved waveguide in the cases of space curved waveguides.

APPENDIX A.

For small values of the step's angle $\delta_p(\sin(\delta_p) \simeq \tan(\delta_p) \simeq \delta_p,\ \cos(\delta_p) \simeq 1)$, condition (2) becomes $\delta_p \geq \sqrt{a^2 + b^2}/(2\pi R)$. For small values of the step's angle, the helical waveguide becomes a toroidal waveguide, where the radius of the curvature of the helix can then be approximated by the radius of the cylinder. In this case, the curved system (x, y, ζ) in conjunction with the curved waveguide is shown in Fig. 1(b), and the transformation of the coordinates Eq. (1) is given as a special case

of the curved transformation of the coordinates, as follows

$$X = (R+x)\cos\left(\frac{\zeta}{R}\right) \quad Y = (R+x)\sin\left(\frac{\zeta}{R}\right) \quad Z = y,$$

and the metric coefficients are given by

$$h_x = 1 \quad h_y = 1 \quad h_\zeta = 1 + \frac{x}{R}.$$

APPENDIX B.

The expression for $\nabla \cdot \mathbf{E}$ is dependent on the metric coefficients as follows

$$\nabla \cdot \mathbf{E} = \mathrm{div}\mathbf{E} = \frac{1}{h_x h_y h_\zeta}\left[\frac{\partial}{\partial x}\left(E_x h_y h_\zeta\right) + \frac{\partial}{\partial y}\left(h_x E_y h_\zeta\right) + \frac{\partial}{\partial \zeta}\left(h_x h_y E_\zeta\right)\right]$$
$$= \frac{1}{h_\zeta}\left[\frac{\partial E_x}{\partial x} h_y h_\zeta + \frac{\partial E_y}{\partial y} h_\zeta + \frac{\partial E_\zeta}{\partial \zeta} h_y + E_x \frac{\partial}{\partial x}\left(h_y h_\zeta\right)\right].$$

The expression for $\nabla \times \mathbf{E}$ is dependent on the metric coefficients as follows

$$\nabla \times \mathbf{E} = \mathrm{curl}\mathbf{E} = \frac{1}{h_x h_y h_\zeta}\begin{bmatrix} h_x\widehat{x} & h_y\widehat{y} & h_\zeta\widehat{\zeta} \\ \frac{\partial}{\partial x} & \frac{\partial}{\partial y} & \frac{\partial}{\partial \zeta} \\ h_x E_x & h_y E_y & h_\zeta E_\zeta \end{bmatrix},$$

and the expression for $\nabla \times (\nabla \times \mathbf{E})$ is given by

$$\nabla \times \left(\nabla \times \mathbf{E}\right) = \frac{1}{h_x h_y h_\zeta}\begin{bmatrix} h_x\widehat{x} & h_y\widehat{y} & h_\zeta\widehat{\zeta} \\ \frac{\partial}{\partial x} & \frac{\partial}{\partial y} & \frac{\partial}{\partial \zeta} \\ h_x\left(\nabla \times \mathbf{E}\right)_x & h_y\left(\nabla \times \mathbf{E}\right)_y & h_\zeta\left(\nabla \times \mathbf{E}\right)_\zeta \end{bmatrix}.$$

REFERENCES

1. Riess, K., "Electromagnetic waves in a bent pipe of rectangular cross section," *Q. Appl. Math.*, Vol. 1, 328–333, 1944.
2. Rice, S. O., "Reflections from circular bends in a rectangular wave guides-matrix theory," *Bell Syst. Tech. J.*, Vol. 27, 305–349, 1948.
3. Cochran, J. A. and R. G. Pecina, "Mode propagation in continuously curved waveguides," *Radio Science*, Vol. 1, No. 6, 679–696, 1966.

4. Carle, P. L., "New accurate and simple equivalent circuit for circular E-plane bends in rectangular waveguide," *Electronics Letters*, Vol. 23, No. 10, 531–532, 1987.
5. Weisshaar, A., S. M. Goodnick, and V. K. Tripathi, "A rigorous and efficient method of moments solution for curved waveguide bends," *IEEE Trans. Microwave Theory Tech.*, Vol. 40, No. 12, 2200–2206, 1992.
6. Cornet, P., R. Duss'eaux, and J. Chandezon, "Wave propagation in curved waveguides of rectangular cross section," *IEEE Trans. Microwave Theory Tech.*, Vol. 47, 965–972, 1999.
7. Heiblum, M. and J. H. Harris, "Analysis of curved optical waveguides by conformal transformation," *IEEE J. Quantum Electron.*, Vol. 11, 75–83, 1975, Correction, Ibid, Vol. 12, 313, 1976.
8. Kawakami, S., M. Miyagi, and S. Nishida, "Bending losses of dielectric slab optical waveguide with double or multiple claddings," *Appl. Optics*, Vol. 14, 2588–2597, 1975, Correction, Ibid, Vol. 15, 1681, 1976.
9. Chang, D. C. and F. S. Barnes, "Reduction of radiation loss in a curved dielectric slab waveguide," *Sci. Rept. 2 AFOSR-72-2417*, 1973.
10. Marcatily, E. A. J. and R. A. Schmeltzer, "Hollow metallic and dielectric waveguides for long distance optical transmission and lasers," *Bell Syst. Tech. J.*, Vol. 43, 1783–1809, 1964.
11. Ghosh, S., P. K. Jain, and B. N. Basu, "Fast-wave analysis of an inhomogeneously-loaded helix enclosed in a cylindrical waveguide," *Progress In Electromagnetics Research*, Vol. 18, 19–43, 1998.
12. Kumar, D. and O. N. Singh II, "Elliptical and circular step-index with conducting helical windings on the core-cladding boundaries for the different winding pitch angles — A comparative modal dispersion analysis," *Progress In Electromagnetics Research*, Vol. 52, 1–21, 2005.
13. Mahmut, A., D. Begum, and K. Yamamoto, "Flow through a helical pipe with rectangular cross-section," *Journal of Naval Architecture and Marine Engineering*, 99–110, 2007.
14. Seshadri, R., S. Ghosh, A. Bhansiwal, S. Kamath, and P. K. Jain, "A simple analysis of helical slow-wave structure loaded by dielectric embedded metal segments for wideband traveling-wave tubes," *Progress In Electromagnetics Research B*, Vol. 20, 303–320, 2010.

15. Ghosh, S., A. K. Sinha, R. K. Gupta, S. N. Joshi, P. K. Jain, and B. N. Basu, "Space-harmonic effects in helical slow-wave structure-An equivalent circuit analysis," *Progress In Electromagnetics Research*, Vol. 30, 85–104, 2001.
16. Lewin, L., D. C. Chang, and E. F. Kuester, *Electromagnetic Waves and Curved Structures*, 95–113, Chap. 8, Peter Peregrinus Ltd., 1977.
17. Trang, N. T. and R. Mittra, "Field profile in a single-mode curved dielectric waveguide of rectangular cross section," *IEEE Trans. Microwave Theory Tech.*, Vol. 29, 1315–1318, 1981.
18. Menachem, Z., "Wave propagation in a curved waveguide with arbitrary dielectric transverse profiles," *Progress In Electromagnetics Research*, Vol. 42, 173–192, 2003.
19. Menachem, Z. and M. Haridim, "Propagation in a helical waveguide with inhomogeneous dielectric profiles in rectangular cross section," *Progress In Electromagnetics Research B*, Vol. 16, 155–188, 2009.
20. Menachem, Z., N. Croitoru, and J. Aboudi, "Improved mode model for infrared wave propagation in a toroidal dielectric waveguide and applications," *Opt. Eng.*, Vol. 41, 2169–2180, 2002.
21. Menachem, Z. and M. Mond, "Infrared wave propagation in a helical waveguide with inhomogeneous cross section and applications," *Progress In Electromagnetics Research*, Vol. 61, 159–192, 2006.
22. Menachem, Z., "Flexible hollow waveguide with two bendings for small values of step angles, and applications," *Progress In Electromagnetics Research B*, Vol. 21, 347–383, 2010.
23. Menachem, Z. and S. Tapuchi, "Helical waveguide with two bendings, and applications," *Progress In Electromagnetics Research B*, Vol. 26, 115–147, 2010.
24. Salzer, H. E., "Orthogonal polynomials arising in the numerical evaluation of inverse Laplace transforms," *Math. Tables and Other Aids to Comut.*, Vol. 9, 164–177, 1955.
25. Salzer, H. E., "Additional formulas and tables for orthogonal polynomials originating from inversion integrals," *J. Math. Phys.*, Vol. 39, 72–86, 1961.
26. The Numerical Algorithms Group (NAG) Ltd., Wilkinson House, Oxford, UK.
27. Collin, R. E., *Foundation for Microwave Engineering*, McGraw-Hill, New York, 1996.
28. Vladimirov, V., *Equations of Mathematical Physics*, 1971.